ARTICLE
https://doi.org/10.26599/AIR.2026.9150009

CAAI Artificial Intelligence Research

Neural Network-Based Fixed-Time Control for Flexible Two-link Manipulators with State Constraints and Input Deadzone

Hejia Gao[124], Tanyu Chen[124], Jiangxu Liu[124], Dengxiang Chang[124], Changyin Sun[1234]

ABSTRACT

Addressing the inherent low stiffness of flexible manipulators, existing control schemes often face an intrinsic contradiction where rapid convergence leads to increased vibration amplitudes, making it challenging to achieve high-precision trajectory tracking while effectively suppressing elastic vibrations. To tackle this issue, this paper proposes a neural network-based Fixed-Time learning control strategy. This strategy is capable of simultaneously handling output constraints, model uncertainties, and input dead-zone nonlinearities of the system. The designed controller effectively compensates for the adverse effects of the input deadzone, ensuring that all system states converge to a small neighborhood around the origin within a fixed time, thereby significantly improving the system's convergence speed and transient performance. By introducing a logarithmic Barrier Lyapunov Function (BLF), the prescribed tracking error constraints are strictly guaranteed. Furthermore, high-frequency chattering is mitigated through a smooth approximation of the sign function. Experimental results demonstrate that, compared with the PSF controller, the proposed Fixed-Time control scheme reduces the steady-state tracking errors by 61.9% and 69.2%, respectively. In terms of vibration suppression, the steady-state values of elastic vibrations are reduced by 49.2% and 32.6%, respectively. These results fully validate the superiority and robustness of the proposed control strategy in balancing rapid convergence with vibration suppression.

KEYWORDS

Vibration control, Flexible manipulator, Fixed-Time control, Input deadzone, Output constraint.

1 Introduction

1.1 Background

With the rapid advancement of robotics technology, flexible manipulators have found widespread application in fields such as deep-sea robotics [1], terrestrial robots [2, 3, 4], and aerospace vehicles [5]. Benefiting from innovations in materials science and upgrades in sensor technology, flexible manipulators possess prominent advantages, including lightweight design and high adaptability. However, the inherent low stiffness of flexible structures also presents unprecedented challenges to their dynamic modeling and precise control, making vibration suppression a core aspect of flexible manipulator control. To fully leverage these advantages, the key lies in integrating artificial intelligence (AI) technology to develop novel modeling methods and control systems tailored to the characteristics of flexible manipulators. Consequently, achieving fast convergence of both tracking errors and vibration amplitudes is of significant practical importance for promoting the real-world application of flexible manipulator technology.

From an engineering perspective, lightweight flexible manipulators are particularly suitable for applications in which low inertia, high payload-to-weight ratio, and energy-efficient motion are required. However, rapid positioning motion can excite elastic modes of the flexible links, resulting in residual vibrations, longer settling times, and reduced end-effector positioning accuracy. These effects may significantly decrease the efficiency and repeatability of practical manipulation tasks. Therefore, achieving rapid trajectory tracking while suppressing elastic vibrations is essential for the reliable application of flexible manipulators in high-speed and high-precision robotic systems.

A flexible manipulator is an underactuated, strongly coupled, and nonlinear system, and its dynamic model is significantly more complex than that of a rigid manipulator. During the control process, elastic vibrations induced by the flexibility of the links make it difficult to achieve superior error convergence. Although partial differential equations (PDEs) can accurately describe the dynamic characteristics of the system, they significantly increase the complexity of control strategies. To reduce the difficulty of control design, the academic community typically employs dimensionality reduction methods to construct dynamic models, such as the Finite Element Method (FEM) [6] and the Assumed Modes

1 School of Artificial Intelligence, Anhui University, Hefei 230601, China
2 Engineering Research Center of Autonomous Unmanned System Technology, Ministry of Education, Hefei, Anhui, China
3 School of Automation, Southeast University, Nanjing 214135, China
4 Anhui Provincial Key Laboratory of Security Artificial Intelligence, Anhui University, Hefei 230601, China
Address correspondence toHejia Gao, hjgao@ahu.edu.cn

Method (AMM) [7]. Most research on vibration control for flexible manipulators adopts AMM for dynamic modeling. In [6], ABAQUS software is utilized to construct a simulation model for the finite element analysis of a flexible gripper. In [8], the AMM is adopted to establish a discretized model for the FTLM. In [9], the AMM is employed to develop the dynamic model of the TLRF manipulator. Therefore, transforming the PDE model into an ordinary differential equation (ODE) model is crucial, as it provides a more convenient foundation for the design of vibration control strategies.

In view of the increasingly widespread application scenarios of flexible manipulators, research on their control strategies holds significant practical importance. In recent years, various methods, such as boundary control [10] and sliding mode control [11], have been applied to the control of flexible manipulator systems. To address the issue that traditional control methods rely excessively on precise dynamic models, model-free control strategies have gradually emerged. Their core advantage lies in the elimination of the need for an accurate dynamic model, relying solely on the input-output data of the control system to achieve favorable control performance in a data-driven manner. Examples of such strategies include PID control [12], fuzzy control [13], and neural network (NN) control [14]. Currently, research on the vibration control of flexible manipulators is extensive [15, 16]. However, the aforementioned studies fail to simultaneously achieve guaranteed transient performance and vibration suppression. Consequently, this paper aims to realize superior vibration suppression while ensuring favorable transient performance.

In addition, actuator input dead zones, tracking-error constraints, and model uncertainties are unavoidable in practical flexible-manipulator systems. The model uncertainties may arise from payload variations, unmodeled flexible modes, and changes in operating conditions, whereas the input dead zone represents a common actuator nonlinearity that reduces the effectiveness of small control commands. The prescribed tracking-error boundaries reflect the positioning-accuracy and operational-safety requirements of practical robotic tasks. If these factors are ignored, the system may exhibit degraded tracking accuracy, increased residual vibrations, longer settling times, or even closed-loop instability[17, 18, 19]. Leveraging their powerful approximation capability for uncertain nonlinear functions, NNs can adaptively compensate for system model uncertainties by dynamically adjusting network weights through online learning, thereby enhancing the system's anti-interference ability and adaptability. Consequently, NN control methods are widely used to address system uncertainties and nonlinearities [20, 21, 22, 23, 24]. In existing research, scholars have proposed various adaptive strategies based on this method. In [25], an adaptive fuzzy NN command-filtered impedance control is proposed to eliminate the influence of unknown system dynamics. For nonlinear multi-agent systems, [26] presents a neural network prescribed-time control method based on a dynamic memory event-triggered mechanism. In [27], an adaptive inverse NN control is presented for uncertain flexible single-link manipulators with input backlash and output constraints. In [28], neural networks are employed to approximate unknown dynamics, and an NN state observer is constructed to compensate for unmeasurable states. In [29], an admittance control strategy based on NN is proposed. In [30], an adaptive NN-based output feedback controller is developed for non-smooth nonlinear systems featuring deadzone and saturation. This paper utilizes the ability of neural networks to approximate nonlinear functions to address the uncertainties and the influence of input deadzone in the flexible manipulator system. To achieve tracking error constraints, a Barrier Lyapunov Function (BLF) is introduced and integrated with the backstepping method to design the controller [31, 32], such as logarithmic, tangent, and integral BLFs.

From a certain perspective, rapid convergence may lead to an increase in the amplitude of elastic vibrations of the manipulator. Consequently, in the presence of input nonlinearities, it is challenging to simultaneously realize excellent error convergence and vibration suppression effects. To achieve high accuracy and rapid convergence, a Fixed-Time controller can serve as a feasible solution. Compared with traditional finite-time control techniques [33], a Fixed-Time control algorithms offer significant advantages in terms of convergence time, as their convergence time is independent of the initial states of the robot and can be predetermined via controller gains [34, 35, 36]. In addition, there are numerous significant research results on Fixed-Time control [37, 38]. In [39], an adaptive fixed-time robust trajectory tracking control strategy is designed for nonlinear robotic manipulator systems subject to friction and external disturbances. In [40], a novel second-order fixed-time sliding mode controller is developed to address mismatched disturbances. In [41], a composite learning fixed-time control strategy is proposed to address the issues of unknown parameters in robotic systems, the difficulty in achieving Fixed-Time convergence for parameter estimation, and the challenge of prespecifying transient performance. In [42], research on the adaptive tracking control problem is conducted within a fixed-time framework for high-order stochastic nonlinear time-delay systems. In [43], an event-triggered super-twisting fixed-time sliding mode consensus control method is proposed for networked nonlinear multi-agent systems with unknown disturbances. However, to the best of our knowledge, research on fixed-time control for flexible two-link manipulators (FTLM) that addresses model uncertainties and input nonlinearities remains relatively scarce.

1.2 Motivation and Contributions

Although existing neural-network-based control methods can compensate for unknown nonlinear dynamics, many of them only guarantee the uniform ultimate boundedness of the closed-loop signals, and the convergence time may depend on the initial conditions. Prescribed-performance control methods can constrain the transient and steady-state tracking errors within predefined envelopes, but they do not necessarily provide a fixed upper bound on the settling time while simultaneously addressing flexible vibration, input dead-zone nonlinearities, and model uncertainties.

To address these limitations, this paper develops a neural-network-based fixed-time control framework for a flexible two-link manipulator subject to model uncertainties, input dead-zone nonlinearities, and state constraints. The novelty does not arise from the individual use of RBF neural networks, fixed-time control, or Barrier Lyapunov Functions, but from their coordinated integration within a unified vibration-control framework. Specifically, two RBF neural-network approximation channels are introduced to compensate for the unknown system dynamics and the input dead-zone nonlinearity, respectively. The fixed-time control structure establishes an explicit upper bound on the convergence time that is independent of the initial conditions, while the logarithmic Barrier Lyapunov Function guarantees that the tracking errors remain within the prescribed boundaries. In addition, a smooth approximation of the sign function is employed to alleviate high-frequency chattering. Inspired by [44], this study improves the controller's dynamic performance by effectively suppressing high-frequency and large-amplitude chattering. The proposed scheme successfully achieves a harmonious optimization between ultra-fast convergence rates and strong robustness, attaining ideal transient response and vibration suppression effects. The following summarizes this paper's main contributions in comparison to earlier research:

- Addressing the limitation of Refs. [37] and [38] in solving only single problems, A unified fixed-time control framework is developed for flexible two-link manipulators subject to model uncertainties, input dead-zone nonlinearities, and state constraints. Different from existing fixed-time methods that mainly focus on convergence analysis or a single type of uncertainty, the proposed method simultaneously considers trajectory tracking, elastic-vibration suppression, unknown dynamics, input nonlinearities, and constrained tracking errors.

- Distinct from the single neural network method in Ref. [37], this paper designs two RBF neural-network approximation channels are introduced to estimate the unknown system dynamics and compensate for the input dead-zone nonlinearity, respectively. Compared with conventional single-network control structures, this design separates the approximation tasks of the two uncertainty sources and reduces the dependence of the controller on an accurate dynamic model.

- A logarithmic Barrier Lyapunov Function is incorporated into the fixed-time control design to guarantee that the tracking errors remain within the prescribed boundaries. Unlike conventional prescribed-performance schemes that mainly regulate the error envelope, the proposed method also provides a fixed upper bound on the convergence time independent of the initial conditions. Moreover, a smooth sign-function approximation is introduced to reduce high-frequency chattering.

The subsequent sections of this paper are organized as follows. Section II presents the preliminary knowledge and system description. Section III presents the controller design and proves its stability. Sections IV and V verify the effectiveness of the controller through simulations and experiments on the Quanser platform, respectively. Finally, Section VI summarizes the contributions of this paper.

2 Dynamic Modeling

2.1 System Description

Based on Hamilton's principle, the dynamic model of the FTLM system is established by incorporating factors such as its rotational inertia, angular velocity, linear velocity, and elastic vibration. This dynamic model is directly adopted in this paper, with detailed derivation procedures referred to in Reference [7]. The FTLM model is derived from the user manual provided by Quanser Inc. [45]. The schematic diagram of the FTLM is shown in Fig. 1, which defines the symbols used in the mathematical modeling of the flexible manipulator. Specifically, XOYZ is an inertial reference frame for determining the spatial position of the manipulator. xoy is a rotational reference frame for observing elastic vibrations. The meanings of each symbol are as follows: τ_i indicates the torque of the i-th drive unit. ω_i represents the elastic vibration of the i-th link in the xoy frame. $Y_i(Q,t)$ is the position of the i-th link. I_{oi} stands for the rotational inertia of the i-th link. I_t is the rotational inertia of the end load. I_{hi} denotes the rotational inertia of the joint. B_i represents the equivalent viscous damping coefficient. K_{si} is the torsional stiffness constant. N denotes the total number of modes.

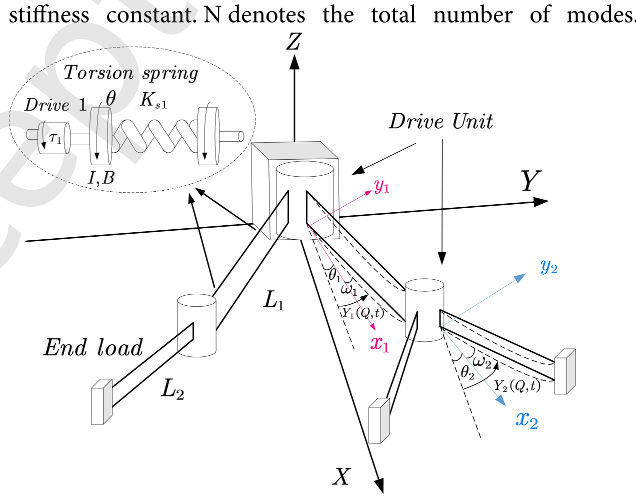

Fig. 1 The Dynamic modeling of FTLM

The state variables of FTLM can be designed as $Q = [\theta, l]^T$. $l = [l_{11}, ..., l_{1n_1}, l_{21}, ..., l_{2n_2}]^T$ is a time-varying generalized coordinate, and $\theta = [\theta_1, \theta_2]^T$ denotes the rotational angles of the links, with $N = n_1 + n_2$. The dynamic equation of the FTLM system is constructed as follows:

$$J(Q)\ddot{Q} + G(Q,\dot{Q})\dot{Q} + F(Q) = N(\tau) \tag{1}$$

where $N(\tau) = \tau - \Delta\tau$ is the deadzone function. The matrices $J(Q)$, $G(Q,\dot{Q})$ respectively are the inertia matrix, Coriolis matrix and centripetal effects, each sized $\mathbb{R}^{(N+2)\times(N+2)}$. $F(Q) \in \mathbb{R}^{N+2}$ is the stiffness matrix. Then, the matrix $Z(Q,\dot{Q})$ designed by $\dot{J}(Q) - 2G(Q,\dot{Q})$ is skew-symmetric. The nonlinear function of the deadzone is

$$N(\tau) = \begin{cases} h(\tau - b_r), & \tau \geq b_r \\ 0, & b_l < \tau < b_r \\ h(\tau - b_l), & \tau \leq b_l \end{cases} \tag{2}$$

Assumption 1: The expected trajectory is smooth, bounded, and continuous.

Assumption1 reflects the fact that practical reference trajectories are normally generated by a trajectory planner or a smooth command filter. More precisely, Q_d, $\dot{Q}_d$, and $\ddot{Q}_d$ are assumed to be bounded, which ensures that the required reference position, velocity, and acceleration are physically realizable. The positive definiteness of $J(Q)$ and the skew-symmetric property of $\dot{J}(Q) - 2G(Q,\dot{Q})$ are standard mechanical properties of Euler–Lagrange robotic systems and hold within the physical operating range of the FTLM. The RBFNN approximation errors $\delta(S)$ and $\delta_\tau(S_\tau)$ are assumed to be bounded only on a compact operating region, which is reasonable because the joint positions, velocities, and actuator inputs of the experimental platform are physically bounded. Furthermore, the BLF design requires the initial tracking error to satisfy $\|f_1(0)\| < k_b(0)$, meaning that the controller is initialized inside the prescribed feasible region.

2.2 Preliminary

Lemma 1 [42]: For any real-valued $c_1, c_2, \ldots, c_n$ with x satisfying $0 \le x \le 1$, the inequality below is applicable.

$$(|c_1| + \cdots + |c_n|)^x \le |c_1|^x + \cdots + |c_n|^x \tag{3}$$

Lemma 2 [38]: Given$u_j > 0$for$k = 1, 2, \ldots, n$, the subsequent inequality is derivable:

$$\left(\sum_{k=1}^{n} u_k\right)^2 = \left(\sum_{k=1}^{n} 1 \cdot u_k\right)^2 \le n \cdot \sum_{k=1}^{n} u_k^2 \tag{4}$$

Lemma 3 [7]: For $x, y \in \mathbb{R}$, $\varepsilon > 0$, $c > 1$, $d > 1$ satisfying $(c-1)(d-1) = 1$, the inequality below is effective:

$$xy \le \frac{\varepsilon^c}{c}|x|^c + \frac{1}{d\varepsilon^d}|y|^d \tag{5}$$

Lemma 4 [42]: Let $\lambda_{\max}(X)$ and $\lambda_{\min}(X)$ denote the maximum and minimum eigenvalues of real matrix$X$. For any$\boldsymbol{m} \in \mathbb{R}^n$ with Euclidean norm $\|\cdot\|$, the inequality holds:

$$\lambda_{\min}(X)\|\boldsymbol{m}\|^2 \le \boldsymbol{m}^{\mathrm{T}} X \boldsymbol{m} \le \lambda_{\max}(X)\|\boldsymbol{m}\|^2 \tag{6}$$

Lemma 5[37]: Consider a dynamical system $\dot{y}(t) = f(t, y)$ with $y(0) = y_0$, $f : \mathbb{R}_+ \times \mathbb{R}^n \to \mathbb{R}^n$, $y \in \mathbb{R}^n$. Assume the origin is the sole equilibrium. If there exists $L(y) > 0$, and for $0 < d < 1$, $\Phi, \Lambda > 0$, $c > 1$, satisfying:

$$\dot{L}(y) \le -\Phi L^c(y) - \Lambda L^d(y) \tag{7}$$

then the origin exhibits fixed-time convergent stability. The settling time T_{Fd} meets the following:

$$T_{Fd} \le T_{\max} = \frac{1}{\Phi(c-1)} + \frac{1}{\Lambda(1-d)} \tag{8}$$

The RBFNN is capable of estimating unknown nonlinear functions and has self-learning capabilities. For a continuous function $g(S) : \mathbb{R}^k \to \mathbb{R}$, the RBFNN is expressed as [29]

$$g(S) = W^T Z(S) \tag{9}$$

where $Z(S) = [z_1(S), z_2(S), \ldots, z_\ell(S)]$ represents the Gaussian basic function, Its component $z_i(S)$ is given as follows

$$z_i(S) = \exp\left[\frac{-(S-\eta_i)^T(S-\eta_i)}{\xi_i^2}\right], \quad i = 1, 2, \ldots, \ell \tag{10}$$

where $\eta_i = [\eta_{i1}, \eta_{i2}, \ldots, \eta_{ik}]$ is the center of the Gaussian basis function. Any continuous function can be estimated by the RBFNN within the compact subset $\Delta_e \subset \mathbb{R}^k$ to arbitrary required precision as

$$g(S) = W^{*T} Z(S) + \epsilon \quad \forall S \in \Delta_e \tag{11}$$

where ϵ represents the bounded approximation error.

3 Control Design

In this section, for the flexible two-link manipulator with unknown robot dynamics, input deadzone, and output constraints, a novel Fixed-Time approach is put forward to realize its trajectory tracking and vibration suppression functions. Specifically, radial basis function neural networks are adopted to approximate the uncertain dynamics and input deadzone nonlinearity, while a logarithmic BLF is introduced to impose constraints on the output states, thereby fulfilling the integrated goals of Fixed-Time trajectory tracking control and flexible vibration suppression for the manipulator. The control block diagram of this Fixed-Time control strategy is shown in Fig. 2.

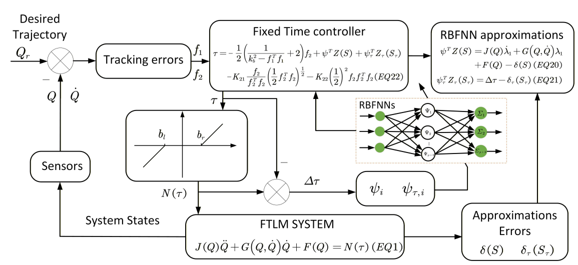

Fig. 2 The control block diagram of the Fixed-Time control

3.1 Fixed-Time Control Design

The tracking error variables $f_1(t)$ and $f_2(t)$ of the FTLM system are constructed as follows

$$f_1(t) = Q - Q_r \tag{12}$$

$$f_2(t) = \dot{Q} - \lambda_1 \tag{13}$$

where λ_1 is the fictitious control variable of $f_1(t)$. By using the inversion method, define virtual control as follows

$$\begin{aligned}\lambda_1 = &-K_{11}\frac{f_1\left(k_b^2 - f_1^T f_1\right)}{f_1^T f_1}\left(\frac{1}{2}\ln\left(\frac{k_b^2}{k_b^2 - f_1^T f_1}\right)\right)^{\frac{1}{2}} \\ &- K_{12}\frac{f_1\left(k_b^2 - f_1^T f_1\right)}{f_1^T f_1}\left(\frac{1}{2}\ln\left(\frac{k_b^2}{k_b^2 - f_1^T f_1}\right)\right)^2 \\ &+ \dot{Q}_d - \left(\frac{1}{2} + \mu\right) f_1\end{aligned} \tag{14}$$

Remark 1: Through computation, the limit of the virtual variable λ_1 exists as $f_1 \rightarrow 0$. Thus, equation (14) is free of singularities, and λ_1 is properly defined for all values of f_1.

Remark 2: Though no singularity arises in (14), the function $f_1/(f_1^T f_1)$ exists within this equation, leading to chattering behavior. To tackle this problem, the function must be approximated in a smooth manner. Inspired by [46], when $f_1/(f_1^T f_1) < v_1$ with v_1 is a positive number, $f_1^T f_1$ is replaced by v_1. Regarding the selection of parameter v_1, it can initially be set to a smaller value, and then modified according to feedback on system performance.

The BLF Lyapunov function is constructed as

$$L_1 = \frac{1}{2} \ln \left(\frac{k_b^2}{k_b^2 - {f_1}^T f_1} \right) \tag{15}$$

where $k_b > 0$ denotes a continuous function, and its role is to implement the constraints on the amplitude of errors. The k_b is defined as

$$k_b = a e^{-\mu t} + b \tag{16}$$

where a, b, and $\mu \geq 0$, and their selection is based on the desired error convergence trajectory.

The constraint boundary should be determined before tuning the remaining controller parameters. It must satisfy $k_b(t) > 0$ and ensure that the initial tracking error lies strictly inside the prescribed region. A smaller value of k_b imposes a tighter tracking-error constraint but may increase the control effort because the denominator of the logarithmic BLF approaches zero near the boundary. For the reported simulation and experiment, constant error boundaries are adopted; therefore, $a = 0$, $b = k_b$, and $\dot{k}_b = 0$. The parameter μ is retained as a nonnegative design coefficient satisfying $|\dot{k}_b/k_b| \leq \mu$ and is tuned together with the virtual-control gains.

The derivative of formula (4) is written as

$$\dot{f}_1 = f_2 + \lambda_1 - \dot{Q}_d \tag{17}$$

The derivative of formula (8) is written as

$$\dot{L}_1 = \frac{{f_1}^T (f_2 + \lambda_1 - \dot{Q}_d) - \frac{\dot{k}_b}{k_b} {f_1}^T f_1}{k_b^2 - {f_1}^T f_1} \tag{18}$$

Considering $f_1^T f_2 \leq \frac{1}{2} f_1^T f_1 + \frac{1}{2} f_2^T f_2$ and $|\dot{k}_b/k_b| \leq \mu$, and substituting (7) into (11), we have

$$\begin{aligned}
\dot{L}_1 \leq & \frac{\frac{1}{2} f_2^T f_2}{k_b^2 - f_1^T f_1} - K_{11} \left(\frac{1}{2} \ln (\frac{k_b^2}{k_b^2 - f_1^T f_1}) \right)^{\frac{1}{2}} \\
& - K_{12} \left(\frac{1}{2} \ln (\frac{k_b^2}{k_b^2 - f_1^T f_1}) \right)^2 \\
\leq & \frac{\frac{1}{2} f_2^T f_2}{k_b^2 - f_1^T f_1} - K_{11} \sqrt{L_1} - K_{12} L_1^2
\end{aligned} \tag{19}$$

Because the dynamic information $J(Q)\dot{\lambda}_1$, $Z(Q,\dot{Q})\lambda_1$, and $P(Q)$ of the robot are unknown, the controllor (19) cannot be used properly. To address this issue, the RBFNN is used to approximate unknown dynamic information. Thus, we have

$$\psi^T Z(S) = J(Q)\dot{\lambda}_1 + G(Q,\dot{Q})\lambda_1 + F(Q) - \delta(S) \tag{20}$$

$$\psi_\tau^T Z(S_\tau) = \Delta\tau - \delta_\tau(S_\tau) \tag{21}$$

where $\psi = [\psi_1, \psi_2, ..., \psi_{N+2}]^T$ and $\psi_\tau = [\psi_1, \psi_2, ..., \psi_{N+2}]^T$ denote the optimal weight,Z(S) is the basis function, $S = \left[Q^T, \dot{Q}^T, \lambda_1^T, \dot{\lambda}_1^T \right]$, $S_\tau = \left[\tau^T, Q^T, \dot{Q}^T, \lambda_1^T \right]$ indicates the input variables of RBFNN, and $\delta(Z) \in \mathbb{R}^{N+2}$ and $\delta_\tau(S_\tau) \in \mathbb{R}^{N+2}$ indicates the approximation error, with the assumption that it is bounded, that is, $||\delta(S)|| \leq \bar{\delta}$ and $||\delta_\tau(S_\tau)|| \leq \bar{\delta}_\tau$ with $\bar{\delta} > 0$ and $\bar{\delta}_\tau > 0$.

The two RBF neural networks have different approximation tasks. The first RBFNN, $\hat{\psi}^T Z(S)$, is used to estimate the unknown model-dependent term $J(Q)\dot{\lambda}_1 + G(Q,\dot{Q})\lambda_1 + F(Q)$, which includes the inertia, Coriolis and centripetal, stiffness, and unmodeled dynamic effects of the flexible manipulator. Its input vector is $S = [Q^T, \dot{Q}^T, \lambda_1^T, \dot{\lambda}_1^T]^T$. The second RBFNN, $\hat{\psi}_\tau^T Z(S_\tau)$, estimates the unknown input loss $\Delta\tau$ introduced by the actuator dead zone, where $N(\tau) = \tau - \Delta\tau$, and its input vector is $S_\tau = [\tau^T, Q^T, \dot{Q}^T, \lambda_1^T]^T$. Consequently, the first network compensates for the unknown system dynamics, whereas the second network compensates for the actuator dead-zone nonlinearity. The bounded terms $\delta(S)$ and $\delta_\tau(S_\tau)$ represent the residual approximation errors and determine part of the final compact convergence set.

Hence, the control torque τ is as follows

$$\begin{aligned}
\tau = & -\frac{1}{2} \left(\frac{1}{k_b^2 - {f_1}^T f_1} + 2 \right) f_2 + \hat{\psi}^T Z(S) + \hat{\psi}_\tau^T Z(S_\tau) \\
& - K_{21} \frac{f_2}{f_2^T f_2} \left(\frac{1}{2} {f_2}^T f_2 \right)^{\frac{1}{2}} - K_{22} \left(\frac{1}{2} \right)^2 f_2 {f_2}^T f_2
\end{aligned} \tag{22}$$

where $K_{21} > 0$ and $K_{22} > 0$ are control gains, and $\hat{\psi}$ represents the estimation of ψ.

Remark 3: Note that the sign function $\frac{f_2}{||f_2||}$ is included in (15), which can cause flutter problems. In this article, the author uses the same smooth approximation sign function as [46]. When $f_2^T f_2 < v_2$ and v_2 is a positive number, $\frac{f_2}{||f_2||}$ is replaced by $\frac{f_2}{\sqrt{v_2}}$. In practice, an initial small value can be chosen for v_2 initially, and then it can be modified based on feedback regarding system performance.

3.2 Stability Analysis

Define

$$L_2 = \frac{1}{2} {f_2}^T J(Q) f_2 \tag{23}$$

The derivative of L_2 is

$$\begin{aligned}
\dot{L}_2 = & {f_2}^T J(Q) \left(J^{-1}(Q)(N(\tau) - G\dot{Q} - F(Q)) - \dot{\lambda}_1 \right) \\
& + \frac{1}{2} f_2^T \dot{J}(Q) f_2
\end{aligned} \tag{24}$$

Then, the matrix $G(Q,\dot{Q})$ designed by $\dot{J}(Q)-2G(Q,\dot{Q})$ exhibits skew-symmetric. Hence, equation (24) can be expressed as follows:

$$\dot{L}_2 = {f_2}^T(\tau - G(Q,\dot{Q})\lambda_1 - F(Q) - J(Q)\dot{\lambda}_1 - \Delta\tau) \tag{25}$$

By substituting Formulas (20), (21) and (22) into (25), we can obtain that

$$\begin{aligned}\dot{L}_2 \le & -\frac{\frac{1}{2}f_2^T f_2}{k_b^2 - f_1^T f_1} - f_2^T f_2 + f_2^T \tilde{\psi}^T Z(S) + f_2^T \tilde{\psi}_\tau^T Z_\tau(S_\tau) \\ & - K_{21}\left(\frac{1}{2}f_2^T f_2\right)^{\frac{1}{2}} - K_{22}\left(\frac{1}{2}f_2^T f_2\right)^2 \\ & - f_2^T \delta(S) - f_2^T \delta_\tau(S_\tau)\end{aligned} \tag{26}$$

From Lemma 4, it follows that

$$-\frac{K_{21}}{\lambda_{\max}^{\frac{1}{2}}(J)}\left(\frac{1}{2}f_2^T J f_2\right)^{\frac{1}{2}} \ge -K_{21}\left(\frac{1}{2}f_2^T f_2\right)^{\frac{1}{2}} \tag{27}$$

$$-\frac{K_{22}}{\lambda_{\max}^2(J)}\left(\frac{1}{2}f_2^T J f_2\right)^2 \ge -K_{22}\left(\frac{1}{2}f_2^T f_2\right)^2 \tag{28}$$

$$f_2^T \delta(S) \le \frac{1}{2}f_2^T f_2 + \frac{1}{2}\delta^T(S)\delta(S) \le \frac{1}{2}f_2^T f_2 + \frac{1}{2}\bar{\delta}^2 \tag{29}$$

Then ,we have

$$\begin{aligned}\dot{L}_2 \le & -\frac{K_{21}}{\lambda_{\max}^{\frac{1}{2}}(J)}\left(\frac{1}{2}f_2^T J f_2\right)^{\frac{1}{2}} - \frac{K_{22}}{\lambda_{\max}^2(J)}\left(\frac{1}{2}f_2^T J f_2\right)^2 \\ & - \frac{\frac{1}{2}f_2^T f_2}{k_p^2 - f_1^T f_1} + f_2^T \tilde{\psi}^T Z(S) + \frac{1}{2}\bar{\delta}^2 \\ & + f_2^T \tilde{\psi}_\tau^T Z_\tau(S_\tau) + \frac{1}{2}\bar{\delta}_\tau^2\end{aligned} \tag{30}$$

Therefore, we can obtain

$$\begin{aligned}\dot{L}_2 \le & -\frac{\frac{1}{2}f_2^T f_2}{k_p^2 - f_1^T f_1} - \frac{K_{21}}{\lambda_{\max}^{\frac{1}{2}}(J)}\sqrt{L_2} - \frac{K_{22}}{\lambda_{\max}^2(J)}L_2^2 \\ & + f_2^T \tilde{\psi}^T Z(S) + f_2^T \tilde{\psi}_\tau^T Z(S_\tau) + \frac{1}{2}\bar{\delta}^2 + \frac{1}{2}\bar{\delta}_\tau^2\end{aligned} \tag{31}$$

where $\tilde{\psi} = \hat{\psi} - \psi$ denotes the error of weight ψ. The NN update laws as follows are constructed:

$$\dot{\hat{\psi}}_i = -\Gamma_i\left[Z_i(S)f_{2i} + \hat{\psi}_i\hat{\psi}_i^T\hat{\psi}_i + \sigma_i\hat{\psi}_i\right] \tag{32}$$

$$\dot{\hat{\psi}}_{\tau,i} = -\Gamma_{\tau,i}\left[Z_{\tau,i}(S)f_{2i} + \hat{\psi}_{\tau,i}\hat{\psi}_{\tau,i}^T\hat{\psi}_{\tau,i} + \sigma_{\tau,i}\hat{\psi}_{\tau,i}\right] \tag{33}$$

where Γ_i and $\Gamma_{\tau,i}$ are constant matrices, and $\sigma_i > 0$ and $\sigma_{\tau,i} > 0, i = 1, 2, ..., N+2$, are the constants. The adaptation matrices Γ_i and $\Gamma_{\tau,i}$ are selected as symmetric positive-definite matrices, and the leakage coefficients satisfy $\sigma_i > 0$ and $\sigma_{\tau,i} > 0$. Increasing Γ_i or $\Gamma_{\tau,i}$ accelerates the corresponding weight adaptation but may amplify measurement noise. The leakage coefficients are introduced to prevent unbounded weight drift. Therefore, these parameters are selected by balancing adaptation speed, robustness, and the residual approximation error. The following Lyapunov function candidates are considered

$$L_3 = \frac{1}{2}\sum_{i=1}^{N+2}\tilde{\psi}_i^T\Gamma_i^{-1}\tilde{\psi}_i \tag{34}$$

$$L_4 = \frac{1}{2}\sum_{i=1}^{N+2}\tilde{\psi}_{\tau,i}^T\Gamma_{\tau,i}^{-1}\tilde{\psi}_{\tau,i} \tag{35}$$

The derivative of L_3 is

$$\begin{aligned}\dot{L}_3 = & -\sum_{i=1}^{N+2}\tilde{\psi}_i^T Z_i(S)f_{2i} - \sum_{i=1}^{N+2}\tilde{\psi}_i^T\hat{\psi}_i\hat{\psi}_i^T\hat{\psi}_i \\ & -\sum_{i=1}^{N+2}\sigma_i\tilde{\psi}_i^T\hat{\psi}_i\end{aligned} \tag{36}$$

By simplifying formula (36) separately, we can obtain

$$\begin{aligned}-\sigma_i\tilde{\psi}_i^T\hat{\psi}_i & \le -\frac{\sigma_i}{2}\tilde{\psi}_i^T\tilde{\psi}_i + \frac{\sigma_i}{2}\psi_i^T\psi_i \\ & \le -\sigma_i\left(\tilde{\psi}_i^T\tilde{\psi}_i\right)^{\frac{1}{2}} + \frac{\sigma_i}{2}\left(\psi_i^T\psi_i + 1\right)\end{aligned} \tag{37}$$

The term $-\tilde{\psi}_i^T\hat{\psi}_i\hat{\psi}_i^T\psi_i$ within formula (36) is simplified to

$$\begin{aligned}-\tilde{\psi}_i^T\hat{\psi}_i\hat{\psi}_i^T\psi_i = & -\|\hat{\psi}_i\|^4 - \|\psi_i\|^2\left(\|\tilde{\psi}_i\|^2 + \tilde{\psi}_i^T\psi_i\right) \\ & - 2\|\tilde{\psi}_i^T\psi_i\|^2 - 3\|\tilde{\psi}_i\|^2\tilde{\psi}_i^T\psi_i\end{aligned} \tag{38}$$

By applying Lemma 3, the term in Formula (38) can be optimized to

$$-3\left\|\tilde{\psi}_i\right\|\tilde{\psi}_i^T\psi_i \le 3\left(\frac{3}{4}\kappa_{1i}^{\frac{3}{4}}\left\|\tilde{\psi}_i\right\|^{\frac{4}{3}} + \frac{1}{4\kappa_{1i}^4}\|\psi_i\|^4\right) \tag{39}$$

$$-\|\psi_i\|^2\tilde{\psi}_i^T\psi_i \le \frac{3}{4}\kappa_{2i}^{\frac{4}{3}}\left(\|\psi_i\|^3\right)^{\frac{4}{3}} + \frac{1}{4\kappa_{2i}^4}\left\|\tilde{\psi}_i\right\|^4 \tag{40}$$

$$-\|\psi_i\|^2\left\|\tilde{\psi}_i\right\|^2 \le -\|\psi_i\|^2\left(2\left\|\tilde{\psi}_i\right\| - 1\right) \tag{41}$$

In addition, it is obvious that $2||\tilde{\psi}_i^T\psi_i||^2 < 0$. According to inequalities (39)-(41) , (38) can be rewritten as

$$\begin{aligned}-\tilde{\psi}_i^T\hat{\psi}_i\hat{\psi}_i^T\hat{\psi}_i \le & -\left(1 - \frac{9}{4}\kappa_{1i}^{\frac{4}{3}} - \frac{1}{4\kappa_{2i}^4}\right)\left\|\tilde{\psi}_i\right\|^4 \\ & - 2\|\psi_i\|^2\left\|\tilde{\psi}_i\right\| \\ & + \left(\frac{3}{4\kappa_{1i}^4} + \frac{4}{3}\kappa_{2i}^{\frac{3}{4}}\right)\|\psi_i\|^4 + \|\psi_i\|^2\end{aligned} \tag{42}$$

Substituting (37) and (42) into (36) yields the following inequality:

$$\begin{aligned}\dot{L}_3 \le & -\sum_{i=1}^{N+2}\tilde{\psi}_i^T Z_i(S)f_{2i} - \sum_{i=1}^{N+2}\left(2\|\psi_i\|^2 + \sigma_i\right)\left(\tilde{\psi}_i^T\tilde{\psi}_i\right)^{\frac{1}{2}} \\ & -\sum_{i=1}^{N+2}\left(1 - \frac{9}{4}\kappa_{1i}^{\frac{4}{3}} - \frac{1}{4\kappa_{2i}^4}\right)\left(\tilde{\psi}_i^T\tilde{\psi}_i\right)^2 + C_1\end{aligned} \tag{43}$$

According to Lemma 4, the expression of (43) is given as

$$\dot{L}_3 \leq -K_{31}\sum_{i=1}^{N+2}\left(\frac{1}{2}\tilde{\psi}_i^T\Gamma_i^{-1}\tilde{\psi}_i\right)^{\frac{1}{2}}-K_{32}\sum_{i=1}^{N+2}\left(\frac{1}{2}\tilde{\psi}_i^T\Gamma_i^{-1}\tilde{\psi}_i\right)^2 - \sum_{i=1}^{N+2}\tilde{\psi}_i^T Z_i(S)f_{2i}+C_1. \tag{44}$$

Based on Lemma 4, the expression of (44) is given as

$$\dot{L}_3 \leq -K_{31}\sqrt{L_3}-\frac{K_{32}}{N+2}L_3^2-\sum_{i=1}^{N+2}\tilde{\psi}_i^T Z_i(S)f_{2i}+C_1 \tag{45}$$

where K_{31}, K_{32}, and C_1 are specified as

$$K_{31}=\min\left\{\frac{\sqrt{2}\left(2\|\psi_i\|^2+\sigma_i\right)}{\sqrt{\lambda_{\max}\left(\Gamma_i^{-1}\right)}},\ i=1,\ldots,N+2\right\} \tag{46}$$

$$K_{32}=\min\left\{\frac{4\left(1-\frac{9}{4}\kappa_{1i}^{\frac{4}{3}}-\frac{1}{4\kappa_{2i}^4}\right)}{\left(\lambda_{\max}\left(\Gamma_i^{-1}\right)\right)^2}, i=1,\ldots,N+2\right\} \tag{47}$$

$$C_1=\sum_{i=1}^{N+2}\left(\left(\frac{3}{4\kappa_{1i}^{\frac{4}{3}}}+\frac{3}{4}\kappa_{2i}^{\frac{4}{3}}\right)\|\psi_i\|^4+\left(1+\frac{\sigma_i}{2}\right)\|\psi_i\|^2+\frac{\sigma_i}{2}\right) \tag{48}$$

Similarly to (36), we can obtain $\dot{L}_4$ as

$$\dot{L}_4 \leq -K_{41}\sqrt{L_4}-\frac{K_{42}}{N+2}L_4^2-\sum_{i=1}^{N+2}\tilde{\psi}_{\tau,i}^T Z_i(S_{\tau,i})f_{2i}+C_2 \tag{49}$$

where K_{41}, K_{42}, and C_2 are specified as

$$K_{41}=\min\left\{\frac{\sqrt{2}\left(2\|\psi_{\tau,i}\|^2+\sigma_{\tau,i}\right)}{\sqrt{\lambda_{\max}\left(\Gamma_{\tau,i}^{-1}\right)}}, i=1,\ldots,N+2\right\} \tag{50}$$

$$K_{42}=\min\left\{\frac{4\left(1-\frac{9}{4}k_{1i}^{\frac{4}{3}}-\frac{1}{4k_{2i}^4}\right)}{\left(\lambda_{\max}\left(\Gamma_{\tau,i}^{-1}\right)\right)^2}, i=1,\ldots,N+2\right\} \tag{51}$$

$$C_2=\sum_{i=1}^{N+2}\left(\left(\frac{3}{4\kappa_{1i}^{\frac{4}{3}}}+\frac{3}{4}\kappa_{2i}^{\frac{4}{3}}\right)\|\psi_{\tau,i}\|^4+\left(1+\frac{\sigma_{\tau,i}}{2}\right)\|\psi_{\tau,i}\|^2+\frac{\sigma_{\tau,i}}{2}\right) \tag{52}$$

To guarantee $K_{32}>0$ and $K_{42}>0$, the auxiliary constants introduced in the Young-inequality analysis are selected such that

$$1-\frac{9}{4}\kappa_{1i}^{4/3}-\frac{1}{4\kappa_{2i}^4}>0, \qquad i=1,\ldots,N+2. \tag{53}$$

These constants are used only in the stability analysis and are not parameters implemented in the controller.

Theorem 1: For the system model in (1), with the controller constructed as (22) and update laws chosen as (32)-(33), consider bounded initial conditions $(Q(0),\dot{Q}(0),\tilde{\psi}(0),\tilde{\psi}_{\tau,i}(0))$, where $Q(0)$ satisfies $f_1(0)\in(-k_b,k_b)$. Then, the signals f_1, f_2, $\tilde{\psi}$, and $\tilde{\psi}_{\tau,i}$ will converge to the sets O_{f_1}, O_{f_2}, $O_{\tilde{\psi}_i}$, and $O_{\tilde{\psi}_{\tau,i}}$ within a fixed time T_{Fd}. The settling time T_{Fd} satisfies the following inequality:

$$T_{Fd}\leq T_{\max}=\frac{2}{\phi_1}+\frac{3}{(1-\Lambda)\phi_2} \tag{54}$$

With $0<\Lambda<1$ being a constant. ϕ_1 and ϕ_2 will be defined subsequently, and O_{f_1}, O_{f_2}, $O_{\tilde{\psi}_i}$, and $O_{\tilde{\psi}_{\tau,i}}$ are defined as

$$O_{f_1}=\left\{f_1\in\mathbb{R}^{N+2}\mid \|f_1\|\leq k_b\sqrt{1-\frac{1}{e^H}}\right\} \tag{55}$$

$$O_{f_2}=\left\{f_2\in\mathbb{R}^{N+2}\mid \|f_2\|\leq\sqrt{\frac{H}{\lambda_{\min}(J(Q))}}\right\} \tag{56}$$

$$O_{\tilde{\psi}}=\left\{\begin{array}{l}\tilde{\psi}=[\tilde{\psi}_1,\tilde{\psi}_2,\ldots,\tilde{\psi}_{N+2}]^T\in\mathbb{R}^{\ell\times(N+2)}\Big| \\ \|\tilde{\psi}_i\|\leq\sqrt{\frac{H}{\lambda_{\min}\left(\Gamma_i^{-1}\right)}},\ i=1,2,\ldots,N+2\end{array}\right\} \tag{57}$$

$$O_{\tilde{\psi}_\tau}=\left\{\begin{array}{l}\tilde{\psi}_\tau=[\tilde{\psi}_{\tau,1},\tilde{\psi}_{\tau,2},\ldots,\tilde{\psi}_{\tau,N+2}]^T\in\mathbb{R}^{\ell\times(N+2)}\Big| \\ \|\tilde{\psi}_{\tau,i}\|\leq\sqrt{\frac{H}{\lambda_{\min}\left(\Gamma_{\tau,i}^{-1}\right)}},\ i=1,2,\ldots,N+2\end{array}\right\} \tag{58}$$

where

$$H=2\sqrt{\frac{3C}{\Lambda\phi_2}} \tag{59}$$

Proof: The Lyapunov function considered is defined as

$$L=L_1+L_2+L_3+L_4 \tag{60}$$

The derivative of L may be expressed as

$$\dot{L}\leq -K_{11}\sqrt{L_1}-\frac{K_{21}}{\sqrt{\lambda_{\max}(J(Q))}}\sqrt{L_2}-K_{31}\sqrt{L_3} - K_{41}\sqrt{L_4}-K_{12}L_1^2-\frac{K_{22}}{\lambda_{\max}^2(J(Q))}L_2^2 - \frac{K_{32}}{N+2}L_3^2-\frac{K_{42}}{N+2}L_4^2+C \tag{61}$$

where

$$C = C_1 + C_2 + \frac{1}{2}\bar{\delta}^2 + \frac{1}{2}\bar{\delta}_\tau^2 \tag{62}$$

Based on Lemma 2, (60) may be rephrased as

$$\dot{L} \leq -\phi_1\sqrt{L} - \frac{\phi_2}{3}L^2 + C \tag{63}$$

where descriptions of ϕ_1 and ϕ_2 are as follows:

$$\phi_1 = \min\left\{K_{11}, \frac{K_{21}}{\sqrt{\lambda_{\max}(J(Q))}}, K_{31}, K_{41}\right\} \tag{64}$$

$$\phi_2 = \min\left\{K_{12}, \frac{K_{22}}{\lambda_{\max}^2(J(Q))}, \frac{K_{32}}{N+2}, \frac{K_{42}}{N+2}\right\} \tag{65}$$

First, the boundedness of all signals in the system needs to be verified. For $L^2 > \frac{3C}{\phi_2}$, $\dot{L} < 0$, leading L to eventually be beneath $\sqrt{\frac{3C}{\phi_2}}$. As the exact scale of L's convergence set cannot be acquired, the convergence set is expanded by the authors to $\{L \,|\, 0 \leq L < \sqrt{\frac{3C}{\phi_2}}\}$. Based on the components of L, f_1, f_2, $\tilde{\psi}$, and $\tilde{\psi}_\tau$ converge to their respective compact sets.

There is a constant $\Lambda \in (0,1)$ satisfying $C \leq \frac{\Lambda\phi_2}{3}L^2$, allowing (50) to be restated as

$$\dot{L} \leq -\phi_1\sqrt{L} - \frac{(1-\Lambda)}{3}\phi_2 L^2 \tag{66}$$

In light of Lemma 5, the convergence of L to $\{L \mid 0 \leq L \leq \sqrt{\frac{3C}{\Lambda\phi_2}}\}$ inside T_{Fd}, with T_{Fd} estimated as:

$$T_{\text{Fd}} \leq T_{\max} = \frac{2}{\phi_1} + \frac{3}{(1-\Lambda)\phi_2} \tag{67}$$

To facilitate stability analysis, a constant H is defined as shown in (58). Taking into account the fact

$$\frac{1}{2}\ln\left(\frac{k_b^2}{k_b^2 - f_1^T f_1}\right) \leq L \tag{68}$$

$$\frac{1}{2} f_2^T J(Q) f_2 \leq L \tag{69}$$

$$\frac{1}{2}\sum_{i=1}^{N+2} \tilde{\psi}_i^T \Gamma_i^{-1} \tilde{\psi}_i \leq L \tag{70}$$

$$\frac{1}{2}\sum_{i=1}^{N+2} \tilde{\psi}_{\tau,i}^T \Gamma_{\tau,i}^{-1} \tilde{\psi}_{\tau,i} \leq L \tag{71}$$

Therefore, derivation shows that f_1, f_2, $\tilde{\psi}$, and $\tilde{\psi}_\tau$ respectively converge into the compact sets $\mathcal{O}_{f_1}$, $\mathcal{O}_{f_2}$, $\mathcal{O}_{\tilde{\psi}}$, and $\mathcal{O}_{\tilde{\psi}_\tau}$ within T_{Fd}.

The above analysis establishes a direct connection between the Lyapunov result and the control objectives. Since $f_1 = Q - Q_r$ and Q contains both the rotational angles and the flexible modal coordinates, the fixed-time convergence of f_1 to a compact neighborhood guarantees trajectory tracking and, when the desired flexible coordinates are set to zero, elastic-vibration suppression. The convergence of $f_2 = \dot{Q} - \lambda_1$ ensures that the system velocity follows the designed virtual control. Moreover, the boundedness of L_1 guarantees that the tracking errors remain strictly within the prescribed BLF boundaries, while the bounded estimation errors $\tilde{\psi}$ and $\tilde{\psi}_\tau$ ensure that all closed-loop signals remain bounded in the presence of unknown dynamics and input dead-zone nonlinearities. According to Eq. (66), these signals enter the corresponding compact sets within

$$T_{\text{Fd}} \leq \frac{2}{\phi_1} + \frac{3}{(1-\Lambda)\phi_2}, \tag{72}$$

where the upper bound is independent of the initial conditions. Therefore, the proposed controller achieves practical fixed-time trajectory tracking, prescribed-error constraint satisfaction, and elastic-vibration suppression, with the residual-set size determined by the bounded neural-network approximation errors.

4 Numerical Simulations

To verify the effectiveness of the Fixed-Time controller, this section conducts simulation validation of trajectory tracking and vibration suppression for the FTLM with unknown dynamics, input deadzone, and output constraints. The PSF controller is selected as the comparison benchmark because it represents a conventional feedback-control strategy with a simple structure and relatively low computational cost. It only uses the measurable joint-position and joint-velocity errors and can therefore be implemented under the same simulation and experimental conditions as the proposed controller. Unlike the proposed method, the PSF controller does not explicitly incorporate fixed-time convergence, neural-network-based uncertainty approximation, input dead-zone compensation, or BLF-based tracking-error constraints. Therefore, comparison with the PSF controller makes it possible to clearly evaluate the additional benefits provided by these mechanisms in terms of tracking accuracy, convergence speed, transient performance, and vibration suppression.

To ensure a fair comparison, the same desired signals, initial conditions, and deadzone function are adopted for both control methods. The reference trajectories are $\theta_{1d} = 15^\circ$ and $\theta_{2d} = 10^\circ$, and the initial states for Q and $\dot{Q}$ are set to zero. The parameters of the deadzone function are defined as $b_r = 1$ and $b_l = -1$.

To quantitatively evaluate the control performance the following key performance indicators are defined. (1) Tracking error which serves to verify the transient performance and accuracy of the system. (2) Vibration suppression amplitude which is used to measure the effectiveness of suppressing elastic vibrations.

4.1 Parameter Configuration

PSF Control

As a conventional baseline, the PSF controller generates the control input directly from the joint-position and joint-velocity errors without introducing an uncertainty approximator, a dead-zone compensator, or an explicit error-constraint mechanism. The form of the partial state feedback control law is

$$\tau_i = -K_1(\theta_i - \theta_{id}) - K_2(\dot{\theta}_i - \dot{\theta}_{id}), i = 1, 2 \quad (73)$$

The PSF control parameters are chosen as $K_1 = [50, 100]^T$ and $K_2 = [0.8, 0.5]^T$.

Fixed-Time Control

Each basis function $S_i(Z)$ in the neural network selects 256 nodes. The center parameters of NN are either -1 or 1, with variances set as $\xi = [4, 4]$ and $\xi_\tau = [2, 2]$. The control parameters are selected as $K_{11} = [40, 30]^T$, $K_{12} = [10, 15]^T$, $K_{21} = [1, 0.1]^T$, $K_{22} = [0.001, 0.01]^T$, $\vartheta_1 = [0.01, 0.001]^T$, $\vartheta_2 = [10, 10]^T$, and $\mu = [0.1, 0.1]^T$. $\Gamma = [100, 100]^T I_{256\times256}$, $\Gamma_\tau = [100, 100]^T I_{256\times256}$, $\sigma = [0.8, 0.5]^T$, $\sigma_\tau = [1, 0.8]^T$. The initial neural network weights $\hat{\psi}_i = \hat{\psi}_{\tau,i} = [0, 0]^T$ $(i = 1, 2, \ldots, 256)$. As the desired trajectory takes the form of a square wave signal, errors will mutate at the square wave transition moments. Therefore, constraint parameters $k_b = [0.6, 0.4]^T$ $\dot{k}_b = [0, 0]^T$) are selected to ensure that the error amplitude does not exceed the limited range.

The controller parameters are selected in the following order. First, the constraint boundary k_b is determined from the allowable tracking-error range and the maximum error caused by the square-wave transitions. Second, positive-definite adaptation matrices and positive leakage coefficients are assigned to guarantee the boundedness of the neural-network weight estimates. Third, the positive gains K_{11}, K_{12}, K_{21}, and K_{22} are tuned according to Eqs. (63)–(66). In particular, K_{11} and K_{21} mainly affect the square-root term in the Lyapunov inequality, whereas K_{12} and K_{22} affect the quadratic term. Increasing these gains improves the convergence rate but may increase the peak control input. Finally, ϑ_1 and ϑ_2 are adjusted to suppress near-origin chattering without introducing excessive smoothing errors.

4.2 Comparison of Simulations Results

The simulation results of the FTLM system under the two controllers are presented in Figs. 3-6. Detailed analysis and evaluation of the trajectory tracking performance and vibration suppression effect of the FTLM system are provided as follows.

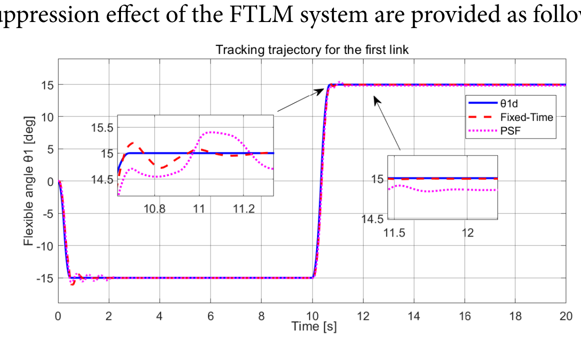

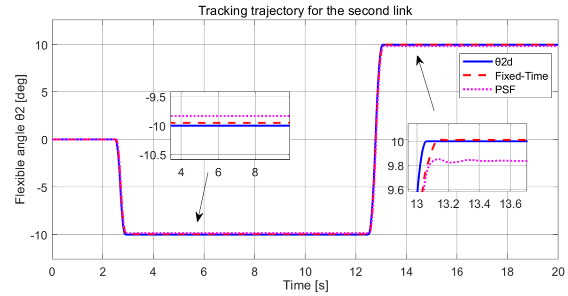

Fig. 3 Simulation results of trajectory tracking under input deadzone

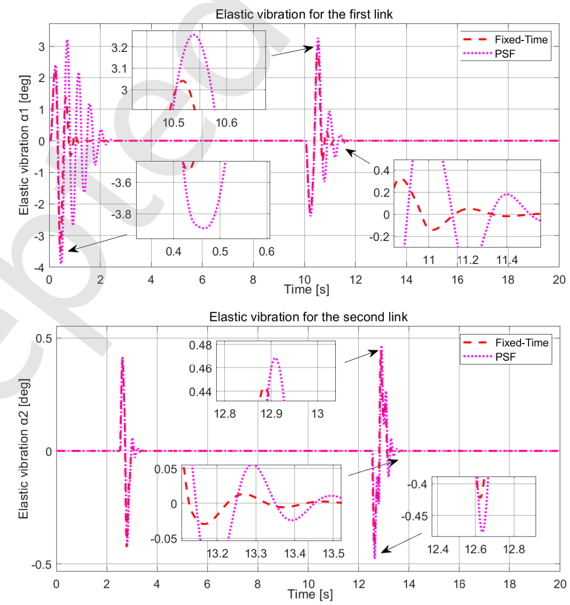

Fig. 4 Simulation results of elastic vibration under input deadzone

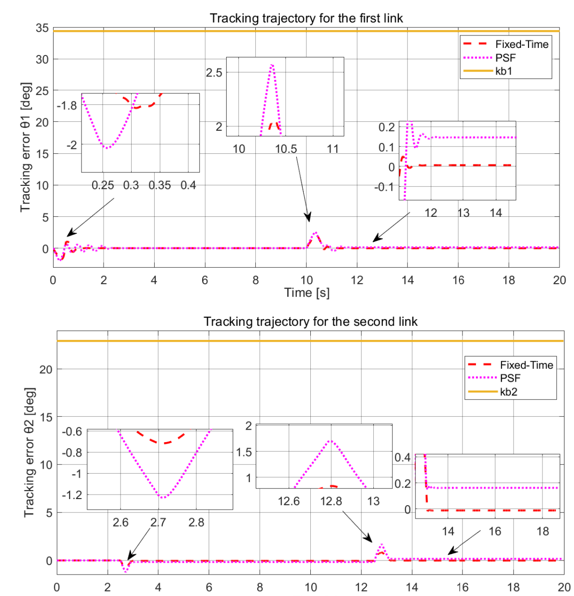

Fig. 5 Simulation results of tracking error under input deadzone

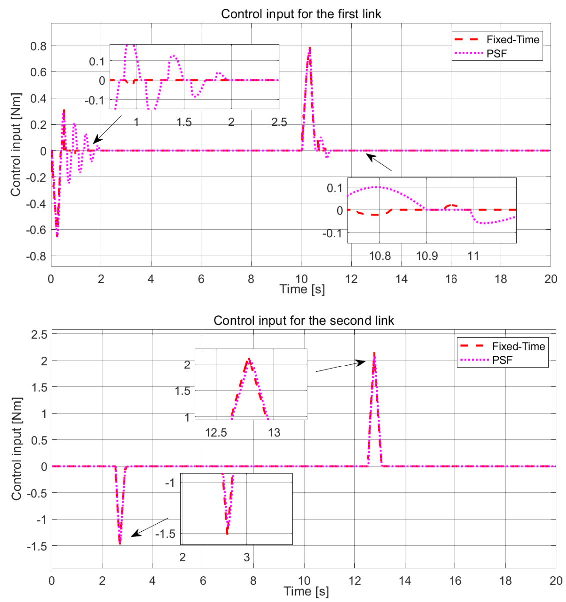

Fig. 6 Simulation results of control input under input deadzone

The trajectory-tracking and tracking-error results are presented in Figs.3 and 5, respectively. Under PSF control, the maximum tracking errors of the first and second links are 2.6° and 1.7°, whereas the corresponding values under the proposed Fixed-Time control are reduced to 2.1° and 0.7°. These results correspond to reductions of approximately 19.2% and 58.8%, respectively. Moreover, the steady-state tracking errors under PSF control are approximately 0.2° for both links, while those under Fixed-Time control approach zero after the transient response. The error peaks mainly occur at the switching instants of the square-wave reference because the desired positions change abruptly. Nevertheless, the tracking errors remain within the prescribed boundaries $k_b = [0.6, 0.4]^T$ rad, corresponding to approximately $[34.4°, 22.9°]^T$. The proposed controller also produces smaller overshoots and faster post-transition error attenuation, demonstrating improved transient and steady-state tracking performance.

Figure.4 presents the elastic-vibration responses of the two links. Under PSF control, the maximum vibration amplitudes of the first and second links are 3.28° and 0.47°, whereas the corresponding values under Fixed-Time control are 3.04° and 0.44°. Thus, the transient vibration peaks are reduced by approximately 7.3% and 6.4%, respectively. More importantly, the vibration curves under the proposed controller decay more rapidly after the square-wave transitions. The vibrations of the two links approach zero at approximately 11.4s and 13.4s, respectively, while noticeable residual oscillations remain under PSF control over the same intervals. This comparison indicates that the proposed controller improves vibration attenuation without sacrificing the rapid tracking response.

The control-input curves are shown in Fig.6. The largest control-input pulses occur near the switching instants of the square-wave reference, when the abrupt tracking-error variation requires rapid acceleration and dead-zone compensation. The peak input magnitudes of the Fixed-Time and PSF controllers are comparable, indicating that the improved tracking and vibration-suppression performance of the proposed method is not achieved through a substantial increase in the maximum control effort. After each transient pulse, the input generated by the proposed controller returns toward zero more rapidly and exhibits no sustained high-frequency oscillation. This behavior also demonstrates the effectiveness of the smooth sign-function approximation in reducing chattering.

Overall, the simulation results demonstrate three main advantages of the proposed method. First, the maximum tracking errors of the two links are reduced from 2.6° and 1.7° under PSF control to 2.1° and 0.7° under Fixed-Time control, corresponding to reductions of approximately 19.2% and 58.8%, respectively. Second, the elastic vibrations decay more rapidly and approach zero at approximately 11.4 s and 13.4 s, while noticeable residual oscillations remain under PSF control. Third, the two controllers have comparable peak control-input magnitudes, but the proposed control inputs return toward zero more rapidly after the reference transitions. These results indicate that the proposed controller improves tracking accuracy and vibration suppression without requiring a substantial increase in the maximum control effort.

In summary, the Fixed-Time control achieves a faster convergence rate. Meanwhile, it exhibits superior trajectory tracking accuracy and vibration suppression performance. By contrast, the PSF control not only has larger steady-state tracking errors but also requires a longer period to suppress elastic vibrations. Additionally, the Fixed-Time control can effectively reduce the system overshoot, further optimizing the transient performance. This fully verifies the effectiveness and practicability of this control strategy.

5 Experimental Results

5.1 Introduction of the Experimental Test Platform

The Quanser flexible system equipment is a high-precision experimental platform, whose core purpose is to support the development and verification of advanced control methods for flexible robotic systems. The Quanser FTLM system is shown in Fig. 7. The first-stage and second-stage links are made of flexible materials with widths of 3 and 1.5 inches, respectively. The FTLM system is powered by two high-precision brushed DC motors, with models Maxon 273759 and 118752, respectively. Angular position measurement is implemented using high-resolution quadrature optical encoders, which have a precision of 1024 lines per revolution, sufficient to meet the strict requirements for position detection. To achieve efficient integration of hardware and control algorithms, the experimental platform adopts a collaborative architecture of QUARC and Simulink software. During the experiment, the data acquisition (DAQ) card is responsible for collecting raw data from sensors and encoders. The power amplifier (AMPAQ) conditions the drive signals. The industrial computer serves as the carrier for algorithm operation, enabling precise control of the FTLM system through the designed control strategy. Next, detailed dynamic parameters of the FTLM system will be provided as shown in Table 1.

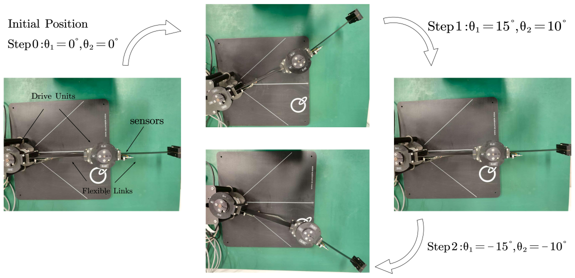

Fig. 7 Experimental equipment diagram of the FTLM

[h]

Table 1 Parameters of the Quanser FTLM planform

Parameters	Link 1	Link 2	Unit
Mass of link	0.49	0.42	kg
Length of link	0.35	0.30	m
Inertia of link	0.02	0.013	kgm^2
Width of link	76.2	38.1	mm
Range of rotation of link	± 90	± 90	deg
Torsional stiffness sonstant	22.0	2.5	N-m/rad
Thickness of link	1.27	0.89	mm
Servomotor torque constant	0.119	0.0234	N-m/A

5.2 Parameter Configuration

The Fixed-Time controller is designed for the FTLM system in this experiment, and this design enables the FTLM to better tackle the disturbances arising from dynamic uncertainties and nonlinearities. Meanwhile, the positioning accuracy of the FTLM is ensured, and its vibrations in the horizontal plane are suppressed. The parameters of the deadzone function are defined as $b_r = 1$ and $b_l = -1$.

1) The PSF control parameters are chosen as $K_1 = [80, 160]^T$ and $K_2 = [1, 2]^T$.

2) The Fixed-Time control parameters are selected as $K_{11} = [20, 60]^T$, $K_{12} = [10, 15]^T$, $K_{21} = [1, 0.1]^T$, $K_{22} = [0.001, 0.001]^T$, $\vartheta_1 = [0.003, 0.001]^T$, $\vartheta_2 = [2, 10]^T$, $\mu = [1, 1]^T$. The neural network parameters are selected as $\Gamma = [5, 10]^T I_{256\times256}$, $\Gamma_\tau = [50, 50]^T I_{256\times256}$, $\sigma = [0.1, 1]^T$, $\sigma_\tau = [1, 0.001]^T$. The constraint parameters are $k_b = [0.5, 0.4]^T$ and $\dot{k}_b = [0, 0]^T$. The remaining parameters are the same as in Section IV.

5.3 Comparison of Experimental Results

In this experiment, a square wave signal with a phase difference of 2.5° is used as the input signal. After conversion and amplification, the signal is applied to the control of the FTLM system. The SRV02 drive system controls the two drive motors respectively, while real-time operating data is collected by sensors to feed back the rotation angle θ and elastic vibration α of the manipulator. Based on this data, the trajectory tracking error is calculated.To verify the effectiveness of the Fixed-Time control scheme, comparative experiments are conducted on the experimental control platform shown in Fig. 7, where the performance of the PSF control and Fixed-Time control algorithms is validated. The experimental results are presented in Figs. 8-11.

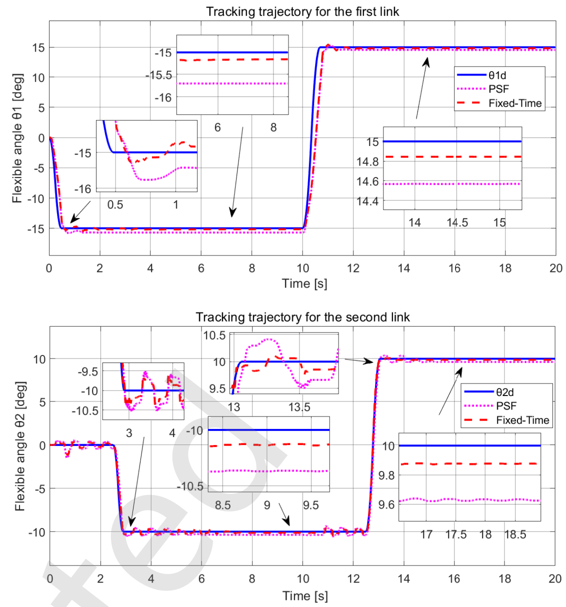

Fig. 8 Experimental results of trajectory tracking under input deadzone

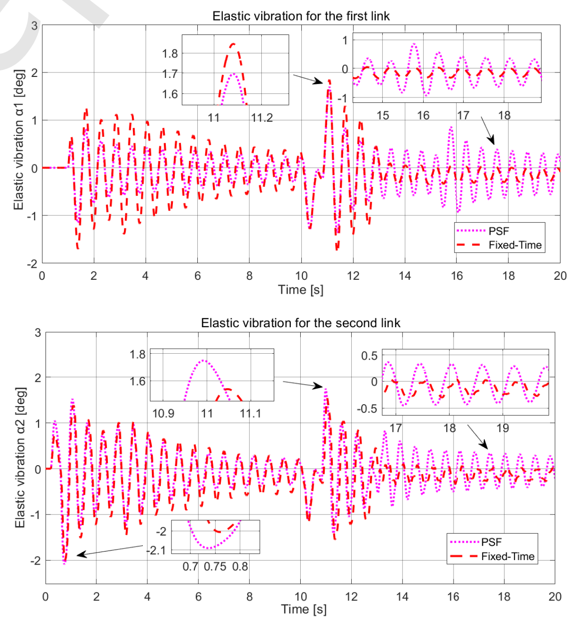

Fig. 9 Experimental results of elastic vibration under input deadzone

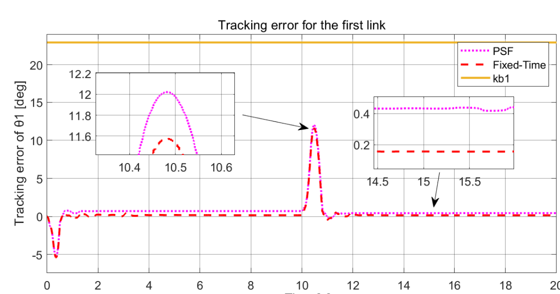

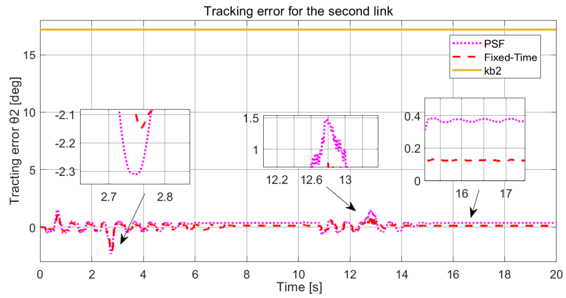

Fig. 10 Experimental results of tracking error under input deadzone

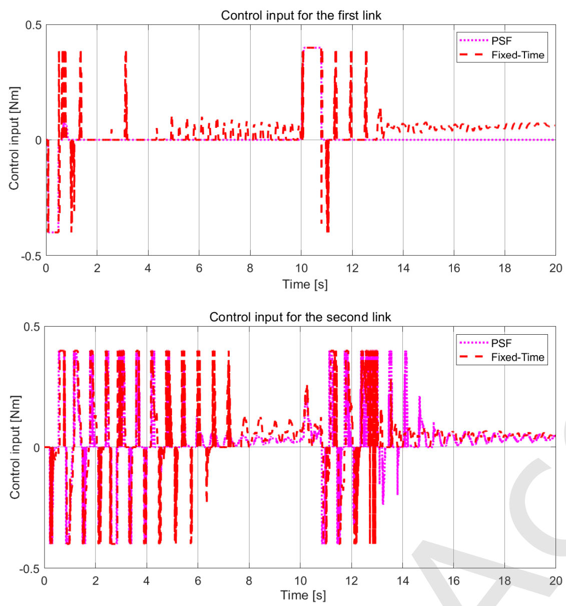

Fig. 11 Experimental results of control input under input deadzone

Table 2 Comparison of the proposed method with PSF control

Methods	Tracking errors (link1/link2)			Vibration(deg)	
	peak-peak value	max value of errors	steady state	peak-peak value	steady state
PSF Control	17.35	12.05	0.42	1.01	0.63
	3.84	1.51	0.39	0.77	0.43
Fixed-Time Control	16.96	11.56	0.16	0.34	0.32
	2.85	0.71	0.12	0.33	0.29

The experimental results of trajectory tracking and tracking errors for the FTLM system are shown in Fig. 8 and Fig. 10, respectively. As can be seen from Fig. 10, under PSF control, the maximum tracking errors of the links are 12.05 and 1.51 deg. Under Fixed-Time control, these values decrease to 11.56 and 0.71 deg. Moreover, the maximum tracking errors of both control strategies do not exceed the preset constraint range k_b, which meets the system error requirements. It can be observed from Fig. 8 that under PSF control, the steady-state tracking errors of the links are 0.42 and 0.39 deg. Under Fixed-Time control, these errors reduce to 0.16 and 0.12 deg. Additionally, the Fixed-Time control exhibits a smaller overshoot and better transient performance.

The elastic vibrations and control inputs of the FTLM system are shown in Fig. 9 and Fig. 11, respectively. The analysis of Fig. 9 demonstrates that the steady-state amplitudes of the elastic vibration of the link under PSF control are 1.01 deg and 0.77 deg, while those under fixed-time control are 0.34 deg and 0.33 deg. Furthermore, the vibrations under Fixed-Time control eventually converge within 0.32 deg and 0.29 deg, whereas the elastic vibrations of the link under PSF control converge within 0.63 deg and 0.43 deg respectively, exhibiting a slower decay rate. Observation of Fig. 11 shows that the control inputs of Fixed-Time control and PSF control are basically equivalent. The former improves performance without significantly increasing control energy consumption.

Table 2 compares the performance of the PSF controller and the Fixed-Time controller in the flexible manipulator system. In terms of trajectory tracking, the peak-to-peak tracking error is reduced by 2.3% and 25.8% with Fixed-Time control compared to PSF control, while the maximum tracking error is reduced by 4.1% and 53%, and the steady-state error by 61.9% and 69.2%. Regarding vibration suppression, the peak-to-peak value of steady-state vibration is reduced by 66.3% and 57.1%, and the steady-state value of elastic vibration by 49.2% and 32.6% under Fixed-Time control compared to PSF control.

In summary, Fixed-Time control exhibits a faster convergence speed and higher trajectory tracking accuracy. It cannot only keep the error of the FTLM system within the set range and improve the system's response efficiency but also enable the elastic vibration to converge with a smaller amplitude and faster speed. In addition, it can effectively reduce the system overshoot to optimize transient performance. In comparison, PSF control has larger steady-state tracking errors and poorer elastic vibration suppression effect. Therefore, the Fixed-Time control strategy proposed in this paper can significantly improve the trajectory tracking performance and vibration suppression efficiency of the FTLM system, which fully verifies its effectiveness.

The experimental results further confirm the advantages observed in the simulations. Compared with PSF control, the proposed controller reduces the steady-state tracking errors of the two links by 61.9% and 69.2%, respectively. The peak-to-peak vibration values are reduced by 66.3% and 57.1%, while the steady-state vibration values are reduced by 49.2% and 32.6%. Moreover, the control-input curves of the two methods have comparable peak ranges and do not exhibit sustained high-frequency oscillations. These improvements are consistent with the roles of the fixed-time terms in accelerating error convergence, the dual RBFNNs in compensating for unknown dynamics and input dead-zone effects, and the logarithmic BLF in maintaining the tracking errors within the prescribed boundaries.

6 CONCLUSIONS

To achieve fast convergence and vibration suppression for the FTLM, this paper proposes a Dual RBFNN-based Fixed-Time Control strategy. The proposed strategy comprehensively addresses critical issues such as system dynamic uncertainties, actuator input deadzones, and output constraints. First, a novel adaptive neural network update law is integrated into the fixed-time control framework. RBFNNs are employed to approximate the unknown dynamics of the flexible manipulator while simultaneously compensating for actuator input dead-zones. Second, large-range oscillations in the control torque are effectively avoided through the smooth approximation of the sign function. Finally, comparative verification with PSF control demonstrates that the proposed Fixed-Time control exhibits superior performance in terms of tracking accuracy and vibration suppression, characterized by smoother transient responses and smaller overshoots. These results fully validate the advantages of the proposed algorithm.

The future work will concentrate on how to further reducing the energy consumption of motors via optimization algorithms while ensuring control performance, such as model predictive path integral control.

Dates

Received: ; Accepted:;
Published online:

References

[1] Guorui Li, Tuck-Whye Wong, Benjamin Shih, Chunyu Guo, Luwen Wang, Jiaqi Liu, Tao Wang, Xiaobo Liu, Jiayao Yan, Baosheng Wu, et al. Bioinspired soft robots for deep-sea exploration. Nature Communications, 14(1):7097, 2023.

[2] Hui Ma, Hongru Ren, Qi Zhou, Hongyi Li, and Zhenyou Wang. Observer-based neural control of n-link flexible-joint robots. IEEE Transactions on Neural Networks and Learning Systems, 35(4):5295–5305, 2022.

[3] Jing Li, Jie Deng, Shijing Zhang, Weiyi Wang, and Yingxiang Liu. An untethered tripodal miniature piezoelectric robot with strong load capacity inspired by land motion of seals. IEEE/ASME Transactions on Mechatronics, 29(1):85–96, 2023.

[4] Xavier Garant and Clément Gosselin. Noncollocated proprioceptive sensing for lightweight flexible robotic manipulators. IEEE/ASME Transactions on Mechatronics, 28(6):3272–3283, 2023.

[5] Zhengwei Wang, Pengfei Wang, Jinjun Duan, and Wei Tian. Review of on-orbit assembly technology with space robots. Aerospace, 12(5):375, 2025.

[6] Haining Xu, Ying Xin, Zihan Wang, Siyi Chen, and Bingheng Li. The design and finite element analysis of the mushroom picking flexible robotic arm. Journal of Vibroengineering, 27(3):550–566, 2025.

[7] Wei He, Hejia Gao, Chen Zhou, Chenguang Yang, and Zhijun Li. Reinforcement learning control of a flexible two-link manipulator: An experimental investigation. IEEE Transactions on Systems, Man, and Cybernetics: Systems, 51(12):7326–7336, 2020.

[8] Hejia Gao, Wei He, Chen Zhou, and Changyin Sun. Neural network control of a two-link flexible robotic manipulator using assumed mode method. IEEE Transactions on Industrial Informatics, 15(2):755–765, 2018.

[9] Qingxin Meng, Xuzhi Lai, Ze Yan, Chun-Yi Su, and Min Wu. Motion planning and adaptive neural tracking control of an uncertain two-link rigid–flexible manipulator with vibration amplitude constraint. IEEE Transactions on Neural Networks and Learning Systems, 33(8):3814–3828, 2021.

[10] Xu Yan, Kun Li, Jiaojiao Zhuang, Chengdong Yang, and Jinde Cao. Boundary control strategies for consensus of fractional-order multi-agent systems based on coupling pde-odes. IEEE Transactions on Circuits and Systems II: Express Briefs, 71(4):2179–2183, 2023.

[11] Deyin Yao, Hongyi Li, and Yang Shi. Event-based average consensus of disturbed mass via fully distributed sliding mode control. IEEE Transactions on Automatic Control, 69(3):2015–2022, 2023.

[12] Di Zhao, Zidong Wang, Shuai Liu, Qing-Long Han, and Guoliang Wei. Pid tracking control under multiple description encoding mechanisms. IEEE Transactions on Systems, Man, and Cybernetics: Systems, 53(11):7025–7037, 2023.

[13] Hang Su, Wen Qi, Jiahao Chen, and Dandan Zhang. Fuzzy approximation-based task-space control of robot manipulators with remote center of motion constraint. IEEE Transactions on Fuzzy Systems, 30(6):1564–1573, 2022.

[14] Yizhuo Sun, Jianxing Liu, Yabin Gao, Zhuang Liu, and Yue Zhao. Adaptive neural tracking control for manipulators with prescribed performance under input saturation. IEEE/ASME Transactions on Mechatronics, 28(2):1037–1046, 2022.

[15] Chen Yang, Qingshuang Wang, Wanze Lu, and Yuanyuan Li. Integrated uncertain optimal design strategy for truss configuration and attitude–vibration control in rigid–flexible coupling structure with interval uncertainties. Nonlinear Dynamics, 113(3):2215–2238, 2025.

[16] Susmita Panda, Arnab Banerjee, and Bappaditya Manna. Design and optimization of inertial amplifier for enhanced vibration control of bridges under moving loads. Applied Mathematical Modelling, 137:115656, 2025.

[17] Yu Zhang, Linghuan Kong, Shuang Zhang, Xinbo Yu, and Yu Liu. Improved sliding mode control for a robotic manipulator with input deadzone and deferred constraint. IEEE Transactions on Systems, Man, and Cybernetics: Systems, 53(12):7814–7826, 2023.

[18] Seungmin Baek, Jongchan Baek, Wookyong Kwon, and Soohee Han. An adaptive model uncertainty estimator using delayed state-based model-free control and its application to robot manipulators. IEEE/ASME Transactions on Mechatronics, 27(6):4573–4584, 2022.

[19] Wansong Liu, Xiao Liang, and Minghui Zheng. Task-constrained motion planning considering uncertainty-informed human motion prediction for human–robot collaborative disassembly. IEEE/ASME Transactions on Mechatronics, 28(4):2056–2063, 2023.

[20] Xingqiang Zhao, Zhen Liu, Baoping Jiang, and Cunchen Gao. Switched controller design for robotic manipulator via neural network-based sliding mode approach. IEEE Transactions on Circuits and Systems II: Express Briefs, 70(2):561–565, 2022.

[21] Huu-Thiet Nguyen and Chien Chern Cheah. Analytic deep neural network-based robot control. IEEE/ASME Transactions on Mechatronics, 27(4):2176–2184, 2022.

[22] Hashim A Hashim and Kyriakos G Vamvoudakis. Adaptive neural network stochastic-filter-based controller for attitude tracking with disturbance rejection. IEEE Transactions on Neural Networks and Learning Systems, 35(1):1217–1227, 2022.

[23] Huanqing Wang, Miao Tong, Xudong Zhao, Ben Niu, and Man Yang. Predefined-time adaptive neural tracking control of switched nonlinear systems. IEEE Transactions on Cybernetics, 53(10):6538–6548, 2022.

[24] Yan Zhang, Jian Guo, and Zhengrong Xiang. Finite-time adaptive neural control for a class of nonlinear systems with asymmetric time-varying full-state constraints. IEEE Transactions on Neural Networks and Learning Systems, 34(12):10154–10163, 2022.

[25] Gang Li, Jinpeng Yu, and Xinkai Chen. Adaptive fuzzy neural network command filtered impedance control of constrained robotic manipulators with disturbance observer. IEEE Transactions on Neural Networks and Learning Systems, 34(8):5171–5180, 2021.

[26] Xiaohong Zheng, Hui Ma, Qi Zhou, and Hongyi Li. Neural-based prescribed-time consensus control for multiagent systems via dynamic memory event-triggered mechanism. Science China Technological Sciences, 68(3):1320402, 2025.

[27] Zhijia Zhao, Kaili Feng, Xiaowei Wang, Chenguang Yang, Xing Li, and Keum-Shik Hong. Adaptive nn control for a flexible manipulator with input backlash and output constraint. IEEE Transactions on Systems, Man, and Cybernetics: Systems, 54(12):7472–7481, 2024.

[28] Boyan Zhu, Hamid Reza Karimi, Liang Zhang, and Xudong Zhao. Neural network-based adaptive reinforcement learning for optimized backstepping tracking control of nonlinear systems with input delay. Applied Intelligence, 55(2):129, 2025.

[29] Hejia Gao, Yang Yang, Jiangxu Liu, and Changyin Sun. Reinforcement learning-based admittance control for physical human-robot interaction with output constraints. IEEE Transactions on Automation Science and Engineering, 22:16334–16345, 2025.

[30] Guangdeng Zong, Qian Xu, Xudong Zhao, Shun-Feng Su, and Limei Song. Output-feedback adaptive neural network control for uncertain nonsmooth nonlinear systems with input deadzone and saturation. IEEE Transactions on Cybernetics, 53(9):5957–5969, 2022.

[31] Rafael Vazquez, Jean Auriol, Federico Bribiesca-Argomedo, and Miroslav Krstic. Backstepping for partial differential equations: A survey. Automatica, 183:112572, 2026.

[32] Dan Bao, Xiaoling Liang, Shuzhi Sam Ge, and Baolin Hou. Adaptive neural trajectory tracking control for n-dof robotic manipulators with state constraints. IEEE Transactions on Industrial Informatics, 19(7):8039–8048, 2022.

[33] Yongling Xia, Yeqing Yuan, and Weichao Sun. Finite-time adaptive fault-tolerant control for robot manipulators with guaranteed transient performance. IEEE Transactions on Industrial Informatics, 21(4):3336–3345, 2025.

[34] Huadi Shan, Yulian Jiang, Yanzheng Zhu, Hongjing Liang, and Shenquan Wang. Fixed-time self-triggered fuzzy adaptive control of n-link robotic manipulators. Fuzzy Sets and Systems, 498:109134, 2025.

[35] Yang Liu, Hongyi Li, Renquan Lu, Zongyu Zuo, and Xiaodi Li. An overview of finite/fixed-time control and its application in engineering systems. IEEE/CAA Journal of Automatica Sinica, 9(12):2106–2120, 2022.

[36] Jorge I Poveda, Miroslav Krstić, and Tamer Başar. Fixed-time nash equilibrium seeking in time-varying networks. IEEE Transactions on Automatic Control, 68(4):1954–1969, 2022.

[37] Wei He, Fengshou Kang, Linghuan Kong, Yanghe Feng, Guangquan Cheng, and Changyin Sun. Vibration control of a constrained two-link flexible robotic manipulator with fixed-time convergence. IEEE Transactions on Cybernetics, 52(7):5973–5983, 2021.

[38] Chengzhi Zhu, Yiming Jiang, and Chenguang Yang. Fixed-time neural control of robot manipulator with global stability and guaranteed transient performance. IEEE Transactions on Industrial Electronics, 70(1):803–812, 2022.

[39] Xin Zhang and Ran Shi. A novel fixed-time stability theorem and its application to nonlinear manipulator trajectory tracking control. International Journal of Robust and Nonlinear Control, 35(11):4712–4723, 2025.

[40] Emmanuel Moulay, Vincent Léchappé, Emmanuel Bernuau, Michael Defoort, and Franck Plestan. Fixed-time sliding mode control with mismatched disturbances. Automatica, 136:110009, 2022.

[41] Shubo Wang, Chuanbin Sun, Qiang Chen, and Haoran He. Composite learning fixed-time control for nonlinear servo systems with state constraints and unknown dynamics. IEEE Transactions on Systems, Man, and Cybernetics: Systems, 55(3):2332–2342, 2025.

[42] Ke Xu, Huanqing Wang, and Peter Xiaoping Liu. Adaptive fixed-time control for high-order stochastic nonlinear time-delay systems: An improved lyapunov–krasovskii function. IEEE Transactions on Cybernetics, 54(2):776–786, 2023.

[43] Guangxin Guo, Haoran Tan, Yun Feng, and Yaonan Wang. Event-triggered super-twisting fixed-time consensus control for networked nonlinear multi-agent systems with disturbance. IEEE Transactions on Automation Science and Engineering, 22:11920 – 11932, 2025.

[44] Guangyu Wu, Jian Sun, and Jie Chen. Optimal linear quadratic regulator of switched systems. IEEE Transactions on Automatic Control, 64(7):2898–2904, 2018.

[45] Quanser. Dynamic equations for the first and second stages of the serial flexible link (dsfl) robot. Maple worksheet or HTML file.

[46] John Y Hung, Weibing Gao, and James C Hung. Variable structure control: A survey. IEEE Transactions on Industrial Electronics, 40(1):2–22, 2002.

Hejia Gao (Member, IEEE) received the B.Eng. degree in intelligence science and technology from the School of Automation and Electrical Engineering, University of Science and Technology Beijing, Beijing, China, in 2016, and the Ph.D. degree in control science and engineering from the School of Automation and Electrical Engineering, University of Science and Technology Beijing, Beijing, China, in 2021. She has been working as a visiting researcher for fifteen months at the Department of Mechanical, Industrial and Aerospace Engineering, Concordia University, Canada, in 2019. Currently, she is working as an associate professor in the School of Artifical Intelligence, Anhui University, Hefei, China. Her research interests include neural networks, RL, flexible systems, and vibration control.

Tanyu Chen received the B.eng degree in China University of Petroleum-Beijing, Beijing, China, in 2023. where he is currently working toward the master's degree in control engineering in the School of Artificial Intelligence, Anhui University, Hefei, China. His research interests include the human-robot Interaction.

Jiangxu Liu received the B.Eng. degree in automation from Zhengzhou University of Light Industry, Zhengzhou, China, in 2023, where he is currently pursuing the master's degree in control engineering with the School of Artificial Intelligence, Anhui University, Hefei, China. His research interests include modeling and intelligent control of flexible manipulator.

Changyin Sun (Senior Member, IEEE) received the B.Eng. degree in applied mathematics from the College of Mathematics, Sichuan University, Chengdu, China, in 1996, and the M.S. and Ph.D. degrees in electrical engineering from Southeast University, Nanjing, China, in 2001 and 2004, respectively. He is currently a Professor with the School of Automation, Southeast University, Nanjing, China. He has co-authored four books and published over 160 international journal papers. Prof. Sun is a Chinese Association of Automation Fellow. He is serving as an Associate Editor of IEEE Transactions on Neural Networks and Learning Systems, Neural Processing Letters, and IEEE/CAA Journal of Automatica Sinica. His research interests include intelligent control, flight control, pattern recognition, and optimal theory.